Finding Discriminative Subgroups of Brain Regions using Tensor Factorization

Yejin Kim, Luca Giancardo, Danilo Pena, Xiaoqian Jiang; for the Alzheimer's Disease Neuroimaging Initiative*
{Yejin.Kim,Luca.Giancardo,Danilo.Pena,Xiaoqian.Jiang}@uth.tmc.edu
University of Texas Health Science Center at Houston
Houston, Texas

ABSTRACT

We developed a supervised tensor factorization approach to identify subgroups of brain regions that are discriminative to patients with Alzheimer's disease (AD), mild cognitive impairment (MCI), and normal controls (CN). The work is a preliminary step to understand the causal relationship between structural brain connectivity in AD. Our model learns from the change of individual brain regions to obtain discriminative sub-graphs, which achieve high AUCs (0.88 for AD vs. MCI, 0.80 for AD vs. CN, and 0.89 for MCI vs. CN).

KEYWORDS

Alzheimer's disease, neuroimaging, brain network, symmetric

ACM Reference Format:
Yejin Kim, Luca Giancardo, Danilo Pena, Xiaoqian Jiang; for the Alzheimer's Disease Neuroimaging Initiative. 2018. Finding Discriminative Subgroups of Brain Regions using Tensor Factorization. In *2019 KDD Workshop on Applied Data Science for Healthcare, August 8, 2019, Anchorage, AK*. ACM, New York, NY, USA, 4 pages. https://doi.org/10.1145/1122445.1122456

1 INTRODUCTION

Alzheimer's disease (AD) is a complex neurodegenerative disorder, and individual patients' degenerative pathological changes over time can vary. Discovery of AD-related biomarkers through magnetic resonance imaging (MRI) is a promising approach to understand AD progression. Many previous studies have investigated structural change caused by atrophy by measuring the loss of brain volume. The brain volume loss is a direct result of loss of neurons, synapses and supporting cellular structures. These MRI-based techniques can also be used as indicators evaluating the risk of future clinical decline [11].

Unfortunately, many of these studies suffer from generalizability and do not emphasize the importance of longitudinal progression patterns [8] [1]. One mitigating strategy is to find robust subgroups of brain regions that are functionally correlated each other. Previous studies use various methods to discover the subgroups, such as community detection [3], principle component analysis [6], and matrix factorization [10]. Meanwhile, one of the most important features that the subgroups should have is discriminability to a clinical outcome of interest. Thus, we aimed to develop a method that can subgroup the brain regions using regional volumes change while ensuring discriminability of the resulting subgroups. We develop a supervised tensor factorization approach that jointly decomposes the volume change into latent space and separates the latent space according to three level of clinical outcomes: AD, mild cognitive impairment (MCI), and normal controls (CN).

2 METHOD

2.1 MRI acquisition and pre-processing

The images were downloaded from the Alzheimer's Disease Neuroimaging Initiative (ADNI) dataset on November 2018. The ADNI was launched in 2003 as a public-private partnership, led by Principal Investigator Michael W. Weiner, MD. The primary goal of ADNI has been to test whether serial MRI, positron emission tomography (PET), other biological markers, and clinical and neuropsychological assessment can be combined to measure the progression of mild cognitive impairment and early Alzheimer's disease.

We selected all of the subjects who had at least 2 T1-weighted acquisitions from the AD, MCI, and CN groups. When a subject had more than two acquisitions, we acquired the first (t_0) and last (t_1) images. The images were processed using the Freesurfer Longitudinal pipeline (v. 6.0) [9] which allows for obtaining a segmentation of cortical and subcortical brain regions, reducing the processing bias due to the selection of a reference time point thanks to a with-in subject template.

There were a total of 971 subjects that had more than one imaging sessions that were greater than six months apart. We did not use any patients that converted from MCI to AD, and all patients were stable within their initial diagnosis for the purposes of this study. As a result, a total of 857 subjects were analyzed for this study.

We extracted 111 brain regions by combining the subcortical segmentation (aseg.stat) and the white matter parcellation (wmparc.stat) files uniquely using the region sizes. Finally, we computed a brain volume matrix $V = \{v_{r,p}\}$ where R represents the brain regions and p represents the patient cohort (AD, MCI, or CN). We computed two brain matrices $V@t_0$ and $V@t_1$, one per time point.

*Data used in preparation of this article were obtained from the AlzheimerâĂŹs Disease Neuroimaging Initiative (ADNI) database (adni.loni.usc.edu). As such, the investigators within the ADNI contributed to the design and implementation of ADNI and/or provided data but did not participate in analysis or writing of this report. A complete listing of ADNI investigators can be found at: *http://adni.loni.usc.edu/wp-content/uploads/how_to_apply/ADNI_Acknowledgement_List.pdf*

DSHealth '19, August 8, 2019, Anchorage, AK, USA

ACM ISBN 978-1-4503-9999-9/18/06…$15.00
https://doi.org/10.1145/1122445.1122456

2.2 Brain volume loss

Using the volume matrices $V@t_0$ and $V@t_1$, we computed brain volume loss during the two time points as our objective is to investigate progressions of neurodegeneration. The decreased volume of brain regions is a direct proxy to cerebral atrophy, which is an important biomarker of the AD and MCI disease states [7].

We first standardized the distribution of volume of each region. That is, for all regions r and for all time steps, $\overline{v_{r,p}} = (v_{r,p} - mean_{v_{r,\cdot}})/\sigma_{v_{r,\cdot}}$, where $mean_{v_{r,\cdot}}$ and $\sigma_{v_{r,\cdot}}$ is mean and standard deviation, respectively. We discard any outliers, which is defined as $|\overline{v_{r,p}}| > 3\sigma_{v_{r,\cdot}}$.

We computed the volume change of 111 brain regions by subtracting the standardized brain volume at t_1 and the brain volume at t_0, i.e., $\delta_{r,p} = \overline{v_{r,p}}@t_1 - \overline{v_{r,p}}@t_0$. We discard any volumetric increase ($\delta > 0$) as it is known that brain regions only shrink, and the increased volume may be due to the procedural limitation of MRI acquisition that cannot distinguish cerebrospinal fluid that fills the empty space after shrinking of neighboring brain regions.

We then calculated the concordant amount of volume loss for each subject and for each pair of regions. That is, for each subject p the concordance value is $o_{p,r_1,r_2} = \delta_{r_1,p} \times \delta_{r_2,p}$ for every pair (r_1, r_2) of brain regions. If region r_1 or region r_2 stay unchanged, their product of volume loss o_{p,r_1,r_2} will be close to zero. If region r_1 and r_2 show volume loss together, then the concordance value will be larger than zero. We hypothesize that this concordance values reflect the underlying mechanism of brain connectivity.

We build a three-order tensor $\mathcal{O}$ with a shape of # subjects × # brain regions × # brain regions that has value o_{p,r_1,r_2} where subject is p and pair of brain regions is (r_1, r_2). The tensor is symmetric in terms of brain regions. The values in the tensor is highly skewed and sometimes a few large values can dominate all the analysis results, so we apply a log transform to the values, i.e., $\log_2(o_{p,r_1,r_2} + 1)$.

2.3 Subgroup of brain regions

Using the tensor that contains volume loss concordance values, we derive subgroups of brain regions that show similar volume loss together. We use tensor factorization (TF) to decompose the volume loss into latent space of brain regions. We also incorporate separating regularizers to encourage subjects (and also brain regions in the end) to be separated according to its disease label (AD, MCI, and CN).

2.3.1 Symmetric non-negative tensor factorization. The most widely used tensor decomposition is CP method [2]. A third-order tensor $\mathcal{O}$ with shape of $I \times J \times K$ is rank-one if it is an outer product of three vectors a, b, c, i.e., $\mathcal{O} = a \circ b \circ c$ where $\circ$ means the vector outer product. o_{ijk}, the element at (i, j, k) in the tensor $\mathcal{O}$, is computed as product of elements in the vector, i.e., $o_{ijk} = a_i b_j c_k$. TF is a dimensionality reduction approach that represents the original tensor as latent dimensions. The CP model approximates the original observed tensor O as a linear combination of rank-one tensors [12]; that is, a third-order tensor $\mathcal{O}$ is decomposed as minimizing difference between observed tensor and approximated tensor as

$$L = ||\mathcal{O} - \sum_{r=1}^{R} a_r \circ b_r \circ c_r||^2 \quad (1)$$

where a positive integer R is the rank, a_r, b_r, c_r are r-th column vectors in matrix A, B, C with shape of $I \times R, J \times R, K \times R$, respectively. Here, A, B, C are called as factor matrices. When tensor $\mathcal{O}$ contains non-negative data (such as intensity), we set non-negative constraints $A, B, C > 0$ for interpretability of latent dimensions, which is so called non-negative tensor factorization (NTF). The observed tensor can contain symmetric data like the pairwise concordance values [2]. This symmetric data needs a decomposition with constraints enforcing the latter two factor matrices B and C for brain regions to be equal $B = C$, so the minimizing objective is

$$L = ||\mathcal{O} - \sum_{r=1}^{R} a_r \circ b_r \circ b_r||^2. \quad (2)$$

2.3.2 Latent space as subgroups. We apply this symmetric NTF to the volume loss concordance values. We let factor matrix A and B represent subjects and brain regions, respectively. The R latent dimensions in factor matrices A and B represent subgroups of related brain regions. Each subgroup consists of a set of brain regions. Individual brain regions contribute to the subgroup with different extent of membership, and the amount of contribution is stored in columns of B. Likewise, individual subjects have characteristics of the R subgroups with different extent of membership, and the amount of membership is stored in rows of A.

2.3.3 Discriminative and compact subgroups. Since our objective is to derive subgroups of brain regions that are discriminative to AD and MCI, we use a discriminative version of TF. This adds separating regularizers that encourage the subgroups to be separated according to the diseases of interest (i.e., AD, MCI, and CN) [5]. Let us say y is a binary indicator vector of AD and MCI (i.e., $AD = 1, MCI = -1$). The factor matrix A contains subjects' membership values to the subgroups. Note that we only use 80% of either AD or MCI patients to train the separating regularizer. With a linear model θ, a hinge loss function to separate AD and MCI is

$$loss_{ADvsMCI} = \max\{0, 1 - y \cdot (A\theta + b)\} + \gamma||\theta||^2 \quad (3)$$

where b is a bias term and γ is a weighting constant for l_2 norm of θ. This model is a linear support vector machine (SVM), which finds a balanced separating plane that discriminate two groups. Similarly, we also separate AD vs CN and MCI vs CN. By jointly optimizing three independent linear SVMs together with TF (i.e., $L + loss_{ADvsMCI} + loss_{ADvsCN} + loss_{MCIvCN}$), we can derive subgroups that are discriminative to all three groups. To further enhance interpretability via compact latent space, we also add l_1 norm regularizer to the factor matrix. The l_1 regularizer shrinks the less important coefficients to zero, as improving interpretability of model: $L + \lambda(||A||_1 + ||B||_1)$ where λ is a weight parameter to balance the tensor error and the $l_1$norm loss.

3 EXPERIMENTS

3.1 Experiment setting

3.1.1 Quantitative evaluation. We evaluated the proposed method in terms of its discriminative power and compactness of the subgroups [5]. We measured the discrimination by the area under the receiver operating characteristic curve (AUC) metric. We computed separate AUC values to classify AD vs CN; MCI vs CN; and AD vs

MCI. We computed the AUCs in two cases: with out-of-bag subjects (i.e., the remaining subjects that are not used to train TF and SVM) and in-bag subjects (i.e., subjects that are used in TF and SVM). The in-bag AUCs are meaningful when the main objective is to discover well-separated subgroups using as much data as possible. The out-of-bag AUCs are also useful to check the generalizability of our supervised regularizer on newly observed data. The out-of-bag AUC is inevitably low as it bears some discrepancy from latent representation in TF and classification error in SVM regularizer.

For interpretability, we measured compactness by sparsity and the degree of overlap between subgroups. The sparsity was computed as the average Gini index of involvement values in each subgroup (i.e., the rows of B) [4]. The overlap measures the degree of overlapping between all subgroups pairs [5]. The overlap is computed as an averaged cosine similarities between all pair of column vectors of B. We also computed mean squared error (MSE) to evaluate how closely the derived subgroups reflect the observed original data. We computed mean and standard deviation after ten repeated trials. We compared the discriminative power and compactness of our proposed method with that of different settings of regularizers:

- TF: Basic symmetric TF model without any regularizers
- TF + SVM: TF with separating regularizers based on SVM
- TF + l_1: TF with l_1-norm regularizer
- TF +l_1- + SVM: TF with l_1-norm and SVM regularizers.

We alternatively optimized TF and SVM. We optimized the SVM every 200 iterations of TF optimization to balance the weight between TF and SVM. The number of subgroups R and the weight on l_1 norm regularizer were selected as 10 and 0.01 after many trials on the training cohort.

3.2 Results

3.2.1 Quantitative performance. We found that our proposed regularized TF outperforms other baselines in terms of discriminative power and compactness. The TF +l_1+SVM shows the highest AUCs, sparsity, and lowest overlap (Table 1). Particularly, the SVM regularizer significantly increased the discriminative power as well as compactness.

3.2.2 Subgroups discovery. We presented the ten subgroups that are derived from the Sym + l_1 norm + SVM. We determined which disease type (e.g. AD, MCI, and CN) the subgroup is significantly correlated with by using the coefficient and p-value of logistic regression (Table 2). We examined the combinations of positive signs of coefficients and p-value < 0.05 from five logistic regression models (AD vs CN; MCI vs CN; AD vs MCI; AD+MCI vs CN; AD vs MCI+CN). We also computed prevalence of the subgroups as the number of subjects whose membership to the subgroup is significantly greater than zero, i.e., $> 10^{-5}$ divided by the total number of populations × 100%. To confirm the discriminability of subgroups, we plotted subject's membership distribution to a certain subgroup across AD, MCI, and CN.

Among the ten subgroups, we found that seven subgroups are significant predictors to classify disease types. For example, a subgroup S3 was a predictor for MCI and mainly consisted of 3rd ventricle and left pallidum (Table 3) with prevalence of 23%. A subgroup S8 was a predictor for AD and MCI, and mainly consisted of non white matter hypointensities and Posterior cingulate cortex (Table 4). The subject's membership distribution also demonstrated the discriminability of S3 and S8 (Fig 1). As the subject's membership

Table 1: Discrimination and compactness comparison.

Task	TF	TF+l_1	TF+SVM	TF+l_1+SVM
AUC (Out-of-bag subjects)				
AD vs CN	0.6284	0.6336	0.575	0.6471
	(0.0501)	(0.0515)	(0.0815)	(0.0433)
MCI vs CN	0.6021	0.6439	0.6199	0.6584
	(0.0278)	(0.0495)	(0.0587)	(0.0373)
AD vs MCI	0.6634	0.7017	0.6838	0.7138
	(0.045)	(0.0453)	(0.0476)	(0.0659)
AUC (In-bag subjects)				
AD vs CN	0.6472	0.6509	0.8674	0.8041
	(0.0283)	(0.0127)	(0.0718)	(0.0849)
MCI vs CN	0.6568	0.6491	0.8884	0.8945
	(0.0139)	(0.0143)	(0.0246)	(0.0246)
AD vs MCI	0.6985	0.6967	0.8415	0.8833
	(0.0194)	(0.0142)	(0.033)	(0.0292)
Interpretability				
Sparsity	0.3583	0.4175	0.3622	0.4
	(0.0048)	(0.0374)	(0.0031)	(0.0263)
Overlap	0.6887	0.6017	0.6936	0.6416
	(0.0086)	(0.0705)	(0.0046)	(0.0491)
MSE	0.0144	0.0148	0.015	0.0151
	(0.0005)	(0.0005)	(0.0004)	(0.0004)

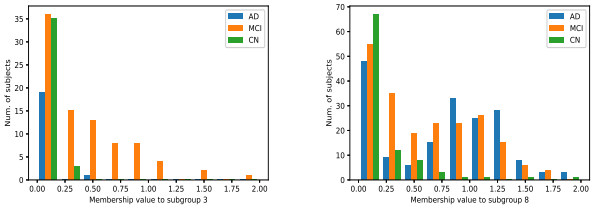

Figure 1: Subject's membership distribution to subgroup S3 and S8.

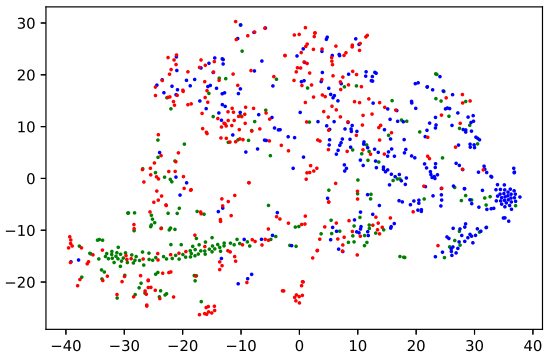

Figure 2: t-sne plot of subject's membership vector (A). Green=AD, Red=MCI, and Blue=CN.

Table 2: Logistic regression coefficient and p-value of the subgroups.

Subgroups	AD vs CN		MCI vs CN		AD vs MCI		AD+MCI vs CN		AD vs MCI+CN		Prevalence	Type
	coef	p-value	coef	p-value	coef	p-value	coef	p-value	coef	p-value		
S1	-3.6696	0.004	0.3721	0.163	-2.0184	0.016	0.2351	0.343	-2.1396	0.012	41.40	MCI+CN
S2	0.0848	0.837	0.0967	0.607	-0.4396	0.109	0.1957	0.287	-0.5367	0.066	68.66	
S3	-6.178	0.093	4.8527	0.001	-9.6557	0	4.5671	0.003	-11.9156	0	23.32	MCI
S4	0.2051	0.752	0.0677	0.658	-0.2261	0.442	0.0917	0.569	-0.3677	0.413	57.43	
S5	-0.2158	0.757	0.1842	0.496	0.1098	0.801	0.3413	0.231	-0.5185	0.327	74.20	
S6	-1.0432	0.085	-0.8137	0.006	-0.2525	0.656	-0.82	0.004	-0.9653	0.074	63.27	CN
S7	6.8306	0.024	2.9858	0.187	2.6628	0.065	4.8454	0.03	3.7964	0.023	21.72	AD
S8	2.9637	0	1.9209	0	0.5498	0	2.8241	0	0.7518	0	76.53	AD+MCI
S9	-1.4285	0.027	0.1717	0.382	-1.4342	0.003	0.2654	0.18	-2.5278	0	77.70	MCI+CN
S10	-4.8927	0	-0.1461	0.603	-2.3311	0.001	-0.2141	0.443	-3.8257	0	62.68	MCI+CN

Table 3: MCI Subgroup S3

Membership	Regions
0.7992	3rd-Ventricle
0.769	Left-Pallidum
0.7421	wm-rh-inferiorparietal
0.5941	Brain-Stem
0.1225	wm-lh-precentral
0.1001	wm-lh-lateralorbitofrontal

Table 4: AD+MCI Subgroup S8

Membership	Regions
0.5545	non-WM-hypointensities
0.3873	CC_Posterior
0.3611	Left-Inf-Lat-Vent
0.3378	Right-Inf-Lat-Vent
0.3337	Right-Pallidum
0.3287	CSF
0.3172	Left-Cerebellum-White-Matter
0.31	CC_Anterior
0.3073	Right-Accumbens-area
0.3038	3rd-Ventricle
0.3028	WM-hypointensities

value to S3 increased, the portion of MCI was increased. Similarly, as the subject's membership value to S8 increased, the portion of AD and MCI increased. We visualized the subject's membership value on the subgroups as a t-sne plot in two dimensions (Fig. 2). There is a clear complex distribution between the MCI and CN patients, whereas the AD patients naturally form their own cluster.

4 CONCLUSION

In this paper, we demonstrated a method that combines tensor factorization to develop latent brain region subgroups that can discriminate AD, MCI and CN patients. These subgroups are computed through volumetric change in brain regions at two different time points which allowed us to understand neurodegenerative patterns over time. This method produced an in-bag AUC of 0.88 (0.03) for the AD vs. MCI classification task. This method can be translated to other neurodegenerative disorders that have a structural volume change over time to detect those who are at high-risk of disease.

REFERENCES

[1] L. M. Aksman, D. J. Lythgoe, S. C. Williams, M. Jokisch, C. Monninghoff, J. Streffer, K. H. Jockel, C. Weimar, and A. F. Marquand. 2016. Making use of longitudinal information in pattern recognition. *Hum Brain Mapp* 37, 12 (12 2016), 4385–4404.

[2] J Douglas Carroll and Jih-Jie Chang. 1970. Analysis of individual differences in multidimensional scaling via an N-way generalization of âĂIJEckart-YoungâĂİ decomposition. *Psychometrika* 35, 3 (1970), 283–319.

[3] Javier O Garcia, Arian Ashourvan, Sarah Muldoon, Jean M Vettel, and Danielle S Bassett. 2018. Applications of community detection techniques to brain graphs: Algorithmic considerations and implications for neural function. *Proc. IEEE* 106, 5 (2018), 846–867.

[4] Niall Hurley and Scott Rickard. 2009. Comparing measures of sparsity. *IEEE Transactions on Information Theory* 55, 10 (2009), 4723–4741.

[5] Yejin Kim, Robert El-Kareh, Jimeng Sun, Hwanjo Yu, and Xiaoqian Jiang. 2017. Discriminative and distinct phenotyping by constrained tensor factorization. *Scientific reports* 7, 1 (2017), 1114.

[6] Nora Leonardi, Jonas Richiardi, Markus Gschwind, Samanta Simioni, Jean-Marie Annoni, Myriam Schluep, Patrik Vuilleumier, and Dimitri Van De Ville. 2013. Principal components of functional connectivity: a new approach to study dynamic brain connectivity during rest. *NeuroImage* 83 (2013), 937–950.

[7] Kelvin K Leung, Jonathan W Bartlett, Josephine Barnes, Emily N Manning, Sebastien Ourselin, Nick C Fox, Alzheimer's Disease Neuroimaging Initiative, et al. 2013. Cerebral atrophy in mild cognitive impairment and Alzheimer disease: rates and acceleration. *Neurology* 80, 7 (2013), 648–654.

[8] S. Rathore, M. Habes, M. A. Iftikhar, A. Shacklett, and C. Davatzikos. 2017. A review on neuroimaging-based classification studies and associated feature extraction methods for Alzheimer's disease and its prodromal stages. *Neuroimage* 155 (07 2017), 530–548.

[9] Martin Reuter, Nicholas J Schmansky, H Diana Rosas, and Bruce Fischl. 2012. Within-subject template estimation for unbiased longitudinal image analysis. *Neuroimage* 61, 4 (2012), 1402–1418.

[10] Aristeidis Sotiras, Susan M Resnick, and Christos Davatzikos. 2015. Finding imaging patterns of structural covariance via non-negative matrix factorization. *Neuroimage* 108 (2015), 1–16.

[11] P. Vemuri, H. J. Wiste, S. D. Weigand, L. M. Shaw, J. Q. Trojanowski, M. W. Weiner, D. S. Knopman, R. C. Petersen, and C. R. Jack. 2009. MRI and CSF biomarkers in normal, MCI, and AD subjects: predicting future clinical change. *Neurology* 73, 4 (Jul 2009), 294–301.